



# Numerical modelling of spontaneous slab breakoff and subsequent topographic response

Thibault Duret<sup>\*</sup>, Taras V. Gerya, Dave A. May

Department of Earth Sciences, Swiss Federal Institute of Technology (ETH Zurich) CH-8092 Zurich, Switzerland

## ARTICLE INFO

### Article history:

Received 2 August 2009

Received in revised form 12 May 2010

Accepted 31 May 2010

Available online 9 June 2010

### Keywords:

Slab breakoff

Slab detachment

Topographic evolution

Peierls creep mechanism

## ABSTRACT

We conducted a set of numerical experiments to study the evolution of a subduction–collision system subject to spontaneous slab breakoff. The study takes into account complex rheological behaviour including plasticity, viscous creep and Peierls creep.

By varying the oceanic slab age and initial plate convergence rate, four different end-members were observed. In this parameter space, breakoff depth can range from 40 to 400 km. Each of those breakoff modes displays complex rheological behaviour during breakoff. Peierls creep in olivine turns out to be a key mechanism for slab breakoff, generally causing slabs to break earlier and at shallower depths.

Models involving different depths of breakoff are subject to different topographic evolution, but always display a sharp breakoff signal. Post breakoff uplift rates in foreland and hinterland basins range between 0.1 km/My for deep detachment and 0.8 km/My for shallow detachment. Our systematic study indicates an approximately linear relationship between the depth of breakoff and the rate of uplift.

Continental crust subduction was observed in breakoff experiments involving oceanic lithosphere older than 30 My. Different exhumation processes such as slab retreat and exhumation occur according to the depth of breakoff. These models are likely to undergo large rebound following breakoff and plate decoupling if the subducted oceanic slab is old enough.

© 2010 Elsevier B.V. All rights reserved.

## 1. Introduction

Slab breakoff, or slab detachment, is often referred to as an early collisional process during which a part of subducted slab detaches from subducting plate. Such a rupture would cause the detached slab to sink down into the Earth's mantle and cause a major thermo-mechanical re-equilibration at the orogen scale. Slowdown of subduction rate is often thought to be the driving mechanism of slab breakoff. Slowdown can be achieved with different scenarios. For example, ridge subduction or subduction of buoyant continental material may strongly decrease subduction rate. This results in large extensive stresses which can then develop in the hanging slab and subsequent slab breakoff can occur.

The concept of slab breakoff comes from the analysis of seismic tomography data where positive seismic velocity anomalies can be observed under collision zones are often interpreted as detached slab segments (Wortel and Spakman, 2000). Many other observations suggest the possibility of slab detachment in subduction–collision setting such as seismicity patterns in subduction zones (Chen and Brudzinski, 2001; Sperner et al., 2001), magmatism geochemistry and surface expression of volcanism (Keskin, 2003; Ferrari, 2004; Qin et al., 2008), uplift data

analysis (Wilmsen et al., 2009) and interpretation of structural and petrological data for exhumation of UHP rocks (Andersen et al., 1991).

Many quantitative slab breakoff studies have already been carried out by means of analytical, semi-analytical, analogue and numerical models, most of those studies involved the evolution of an already subducted slab (Davies and von Blanckenburg, 1995; Ton and Wortel, 1997; van de Zedde and Wortel, 2001; Buitter et al., 2002; Li and Liao, 2002; Cloetingh et al., 2004; Gerya et al., 2004; Toussaint et al., 2004; Macera et al., 2008; Regard et al., 2008; Andrews and Billen, 2009).

Those studies propose different depth ranges where slab breakoff could occur. In van de Zedde and Wortel (2001) detachment occurs at shallow depths (~35 km), in Gerya et al. (2004) detachment occurs at depths greater than 100 km. On the other hand, Andrews and Billen (2009) predict different breakoff depth ranges related to different mechanisms. They introduce two categories of slab breakoff: a shallow breakoff mode (~150 km) involving a weak slab and fast plastic yielding, and a deep (~300 km) breakoff mode involving stronger slabs characterised by slow thermal yielding.

In contrast with preceding studies, Baumann et al. (2010) used a different setup allowing spontaneous slab detachment after a period of oceanic subduction including the effects of phase transitions. In this study breakoff depths ranged between 400 and 600 km.

Few studies quantitatively examined the topographic response to slab detachment. Buitter et al. (2002) predicted topography uplift in the range of 2 to 6 km using an elastic model whereas Gerya et al.

<sup>\*</sup> Corresponding author. Tel.: +41 44 632 30 88.

E-mail address: [Thibault.Duret@erdw.ethz.ch](mailto:Thibault.Duret@erdw.ethz.ch) (T. Duret).

**Table 1**

Rheological parameters of materials used for the experiments.  $\eta$  is the reference viscosity,  $n$  is the stress exponent,  $E_a$  is the activation energy,  $V_a$  is the activation volume,  $\phi$  is the friction angle, and  $C$  is the cohesion. Parameters used for Peierls mechanism are  $A_{Peierls} = 10^{7.8} \times 10^{-12}$ ,  $\sigma_{Peierls} = 2.9$  GPa for wet olivine rheology (Katayama and Karato, 2008), and  $\sigma_{Peierls} = 9.1$  GPa for dry olivine rheology (Evans and Goetze, 1979).

Material	Flow law	$\eta(\text{Pa}^n \cdot \text{s})$	$n$	$E_a(\text{J})$	$V_a(\text{J}/\text{bar})$	$\sin(\phi)$	$C(\text{MPa})$
Sediments	Wet quartzite	$1.97 \times 10^{17}$	2.3	$1.54 \times 10^5$	0.8	0.15	1
Upper continental crust	Wet quartzite	$1.97 \times 10^{17}$	2.3	$1.54 \times 10^5$	0.8	0.15	1
Lower continental crust	Plagioclase (An75)	$4.80 \times 10^{22}$	3.2	$2.38 \times 10^5$	1.2	0.15	1
Upper oceanic crust	Wet quartzite	$1.97 \times 10^{17}$	2.3	$1.54 \times 10^5$	0.8	0.00	1
Lower oceanic crust	Plagioclase (An75)	$4.80 \times 10^{22}$	3.2	$2.38 \times 10^5$	0.8	0.60	1
Mantle	Dry olivine	$3.98 \times 10^{16}$	3.5	$5.32 \times 10^5$	0.8	0.60	1
Weak zone	Wet olivine	$5.01 \times 10^{20}$	4.0	$4.70 \times 10^5$	0.8	0.00	1

(2004) predicted lower uplift values (<2 km) using a visco-plastic model.

In this paper, we examine a set of spontaneous slab breakoff numerical experiments using a similar approach to Baumann et al. (2010). We focused the study on the effect of oceanic plate age and convergence rate on slab breakoff, whilst taking into account complex rheological behaviour including Peierls mechanism (Kameyama et al., 1999). Our intent is to (i) identify different slab breakoff modes and characterise the rheological mechanisms responsible for each end-member, and (ii) describe the topographic evolution and orogenic development above a collisional zone subject to slab breakoff.

**2. Model setup**

*2.1. Numerical code description*

The numerical experiments were conducted in two dimensions using the thermo-mechanical code I2VIS (Gerya and Yuen, 2003a). This numerical code is based on conservative finite differences and non-

**Table 2**

Thermal parameters of materials used for the experiments. Temperature dependent thermal conductivity  $k$  is documented in (Clauser and Huenges, 1995).  $H_r$  is the radioactive heat production and  $C_p$  is the isobaric heat capacity.

Material	$k(\text{W}/\text{m}/\text{K})$	$H_r(\text{W}/\text{m}^3)$	$C_p(\text{J}/\text{kg})$
Sediments	$0.64 + \frac{807}{T+77}$	$1.50 \times 10^{-6}$	1000
Upper continental crust	$0.64 + \frac{807}{T+77}$	$1.00 \times 10^{-6}$	1000
Lower continental crust	$1.18 + \frac{474}{T+77}$	$0.25 \times 10^{-6}$	1000
Upper oceanic crust	$0.64 + \frac{807}{T+77}$	$0.25 \times 10^{-6}$	1000
Lower oceanic crust	$1.18 + \frac{474}{T+77}$	$0.25 \times 10^{-6}$	1000
Mantle	$0.73 + \frac{1293}{T+77}$	$2.20 \times 10^{-8}$	1000
Weak zone	$0.73 + \frac{1293}{T+77}$	$2.20 \times 10^{-8}$	1000

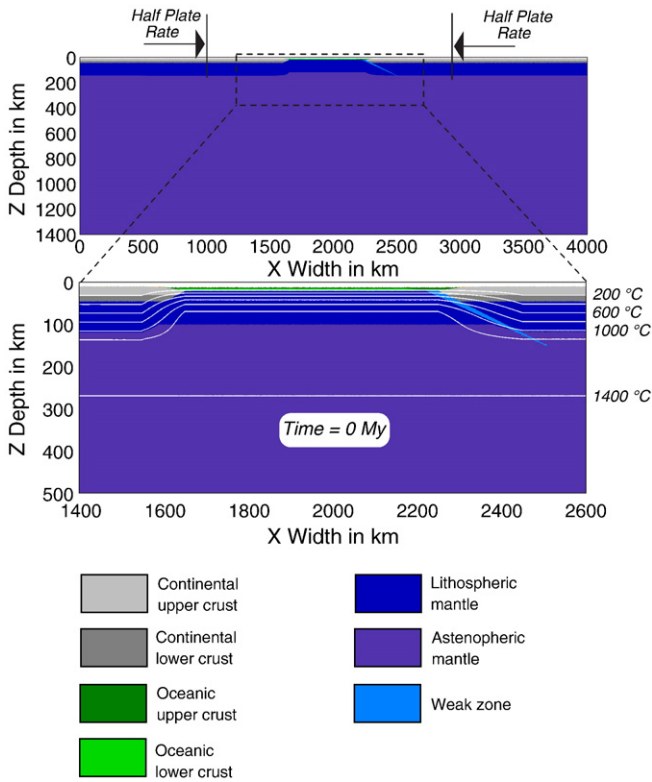


**Fig. 1.** Description of the model box used for the experiments. Full box initial geometry and crop on the oceanic segment with initial thermal structure (plate age = 20 My). Initial plate rate are applied at  $x = 1000$  km for the left plate and  $x = 3000$  km for the right plate.

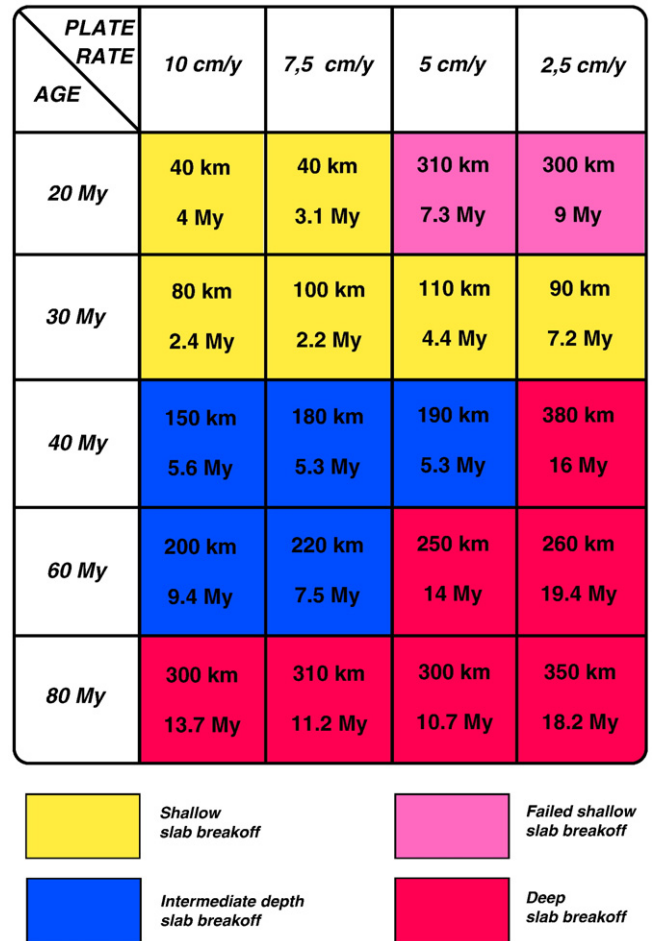


**Fig. 2.** Description of the results of the parametric study. Discrimination of four different end-members, depths of breakoff and time of breakoff for each experiment. Time of breakoff is incremented after forced convergence is stopped.

diffusive marker-in-cell technique taking into account visco-plastic rheologies. Both 2D Stokes flow and continuity equations are solved on a staggered finite difference grid. The system of equation takes the form:

$$\frac{\partial \sigma_{xx}}{\partial x} + \frac{\partial \sigma_{xz}}{\partial z} = \frac{\partial P}{\partial x} \quad (1)$$

$$\frac{\partial \sigma_{zz}}{\partial z} + \frac{\partial \sigma_{zx}}{\partial x} = \frac{\partial P}{\partial z} - g\rho(T, P, C, M) \quad (2)$$

$$\frac{\partial v_x}{\partial x} + \frac{\partial v_z}{\partial z} = 0 \quad (3)$$

In Eqs. (1) and (2),  $\sigma_{xx}$ ,  $\sigma_{zz}$ ,  $\sigma_{xz}$  are the deviatoric stress tensor components. The density  $\rho$  is an explicit function of the temperature ( $T$ ),

the pressure ( $P$ ), the composition ( $C$ ) and the mineralogy ( $M$ ). The heat equation is solved in a Lagrangian manner and is expressed in the following way:

$$\rho C_p \frac{DT}{Dt} = -\frac{\partial q_x}{\partial x} - \frac{\partial q_z}{\partial z} + H_r + H_T + H_s \quad (4)$$

$$q_x = -k(T, C) \frac{\partial T}{\partial x} \quad (5)$$

$$q_z = -k(T, C) \frac{\partial T}{\partial z} \quad (6)$$

$$H_T = \left(1 - \rho \left(\frac{\partial H}{\partial P}\right)_T\right) \frac{DP}{Dt} \quad (7)$$

$$H_s = \sigma_{xx} \dot{\epsilon}_{xx} + \sigma_{zz} \dot{\epsilon}_{zz} + \sigma_{xz} \dot{\epsilon}_{xz} \quad (8)$$

$$C_p = \left(\frac{\partial H}{\partial T}\right)_P \quad (9)$$

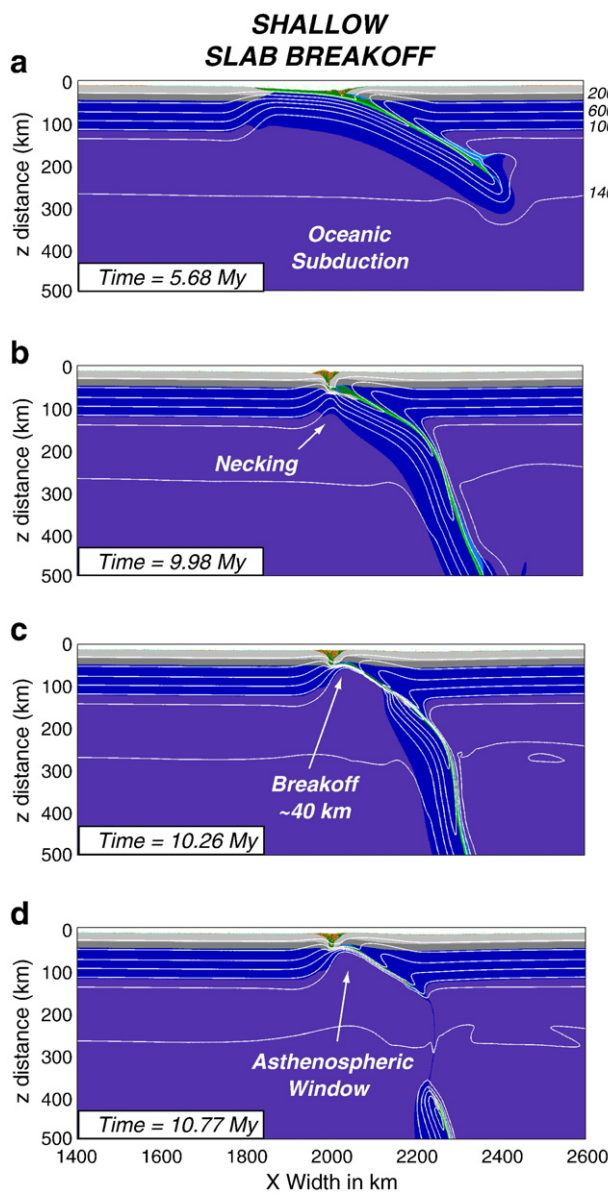


**Fig. 3.** Four stages evolution of the shallow slab breakoff end-member. a) Oceanic subduction. b) Continental collision, necking in the mantle lithosphere. c) Breakoff d) Post breakoff rebound and asthenospheric window. Time is incremented from the start of the experiment. Origin of the z distance axis is the top of the box (including the 10 km thick air layer).

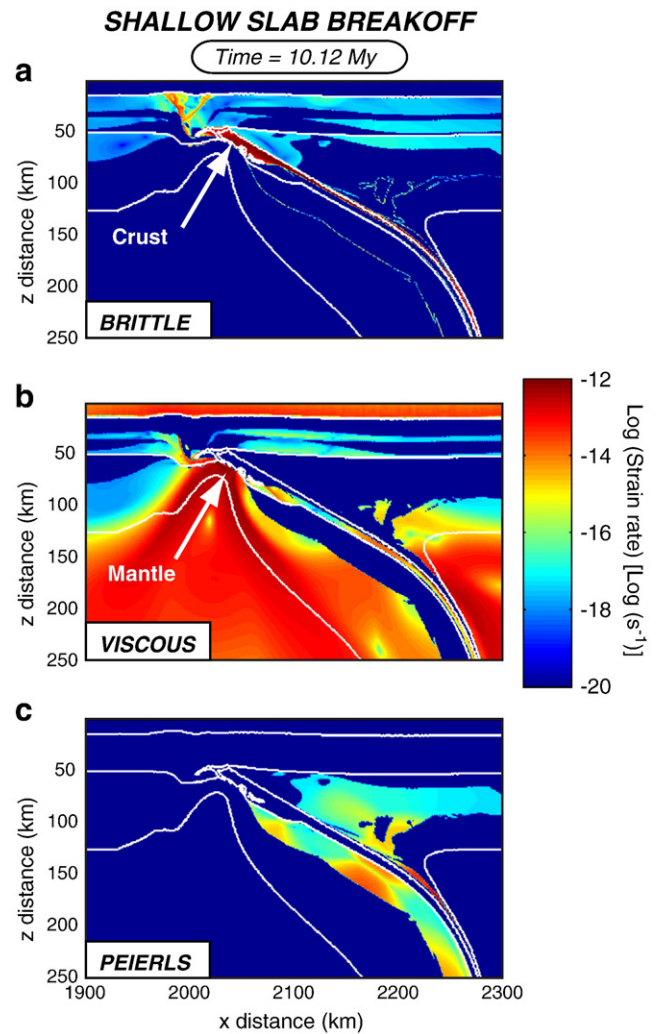


**Fig. 4.** Rheological mechanisms activated during shallow slab breakoff. Brittle, viscous, and Peierls mechanism strain rates. At breakoff location, the crust deforms in a plastic manner (brittle) and the mantle lithosphere deforms viscously. Dark blue means that mechanism is locally not activated during the process. Contours highlight interfaces between atmosphere, crust, mantle lithosphere and asthenosphere.

Such a formulation takes into account the effect of radioactive heating ( $H_r$ ), isothermal compression/decompression effects ( $H_T$ ), shear heating ( $H_s$ ). Thermal conductivity  $k(T, C)$  is a function of both temperature and composition (cf. Table 1).  $q_x$  and  $q_z$  are the components of the heat flux vector,  $\dot{\epsilon}_{xx}$ ,  $\dot{\epsilon}_{zz}$ ,  $\dot{\epsilon}_{xz}$  are the components of the strain rate tensor,  $H$  is the rock enthalpy at the current timestep. The isobaric heat capacity ( $C_p$ ) and isothermal compression term are computed at each timestep and takes into account the effect of latent heat due to phase transformations. Evaluation of  $H_T$  and  $H_s$  terms requires information from the pressure and stress tensor components. These terms are thus computed after solving Stokes equations. The heat equation can then be solved taking into account the effect of isothermal compression, phases changes and shear heating at the current timestep. All the local rock properties (density, heat capacity, and thermal expansion) are updated at each timestep according to Gibbs energy minimisation. (Gerya et al., 2004; Baumann et al., 2010).

The rheologies used in the experiments are visco-plastic. Viscous creep is computed in terms of deformation invariants and depends on strain rate, temperature, and pressure (Ranalli, 1995). The viscous component of the deformation is calculated as a combination of diffusion ( $\eta_{diff}$ ) and dislocation creep ( $\eta_{disc}$ ).

$$\frac{1}{\eta_{creep}} = \frac{1}{\eta_{diff}} + \frac{1}{\eta_{disc}} \quad (10)$$

The calculation of the viscosity associated with dislocation creep regime is formulated as follows:

$$\eta_{creep} = (\dot{\epsilon}_{II})^{(1-n)/2n} (A)^{-1/n} \times e^{\left(\frac{E_a + PV_a}{nRT}\right)} \quad (11)$$

where  $\dot{\epsilon}_{II}$  is the second invariant of strain rate,  $A$ ,  $E_a$ ,  $V_a$ ,  $n$  are respectively, a material constant, the activation energy, the activation volume, and the stress exponent. Those material properties are determined from laboratory flow experiments and are given in Table 1. Variations of flow parameters (activation volume) with phase transitions are not included. A smooth transition between diffusion creep and dislocation creep is assumed to occur at approximately 30 kPa (Turcotte and Schubert, 1982). By equating strain rate invariants for dislocation creep and diffusion creep at the stress transition, an expression for diffusion creep viscosity is derived as a function of the dislocation creep flow law.

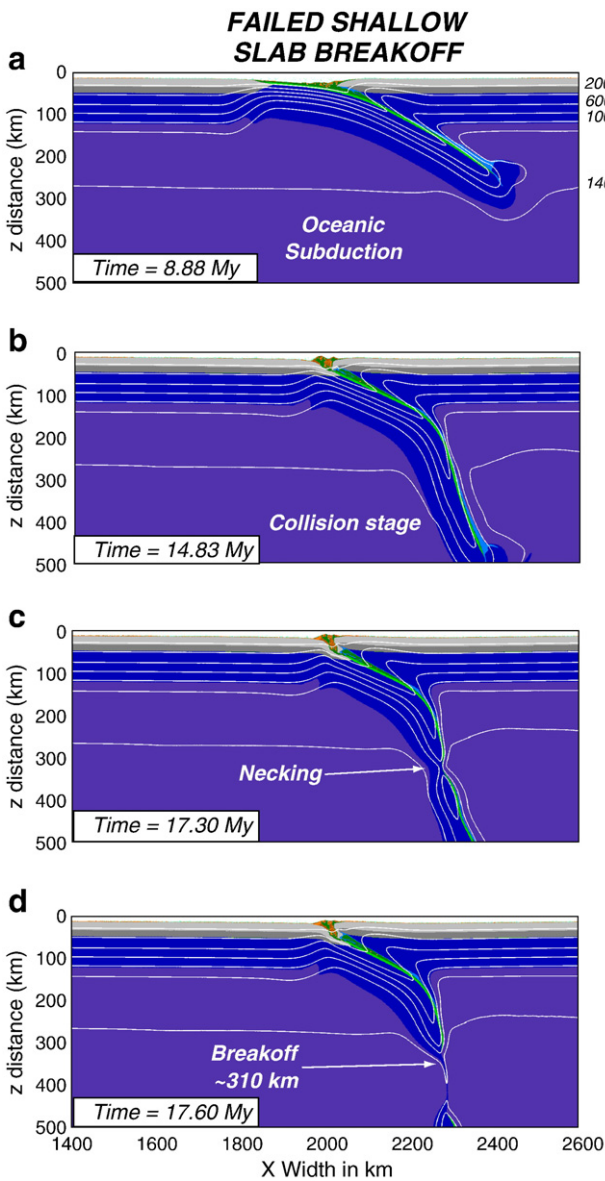


**Fig. 5.** Evolution of the failed shallow slab breakoff end-member. a) Oceanic subduction. b) Continental collision. c) Necking of the slab d) Breakoff and rebound. Time is incremented from the start of the experiment. Origin of the z distance axis is the top of the box (including the 10 km thick air layer).

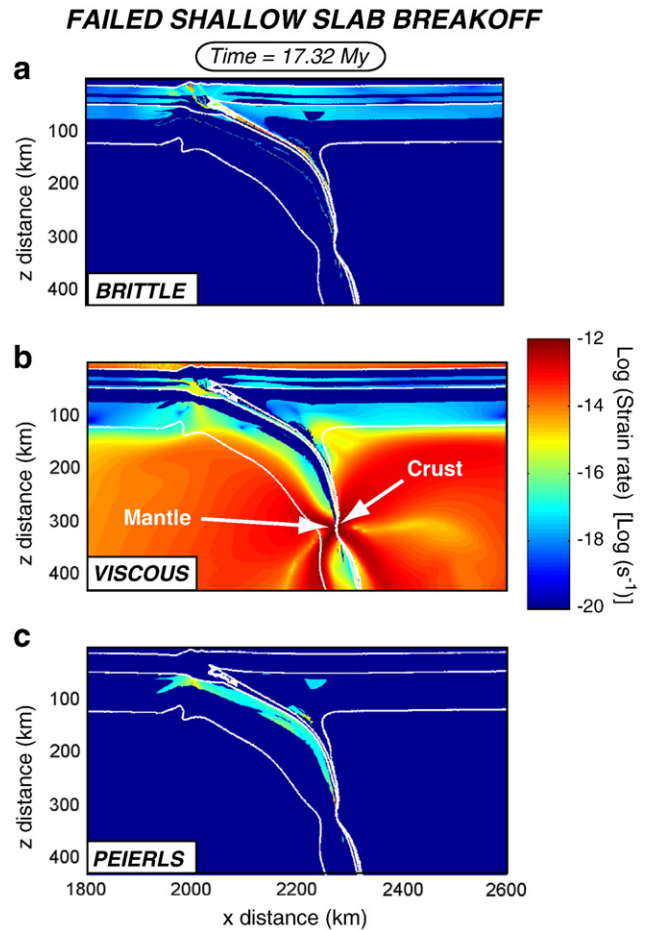


**Fig. 6.** Rheological mechanisms activated during failed shallow slab breakoff. Brittle, viscous, and Peierls mechanism strain rates. At breakoff location, the crust and mantle lithosphere deform viscously. Dark blue means that a mechanism is locally not activated during the process. Contours highlight interfaces between atmosphere, crust, mantle lithosphere and asthenosphere.

Plasticity is implemented using the Druker–Prager yield criterion (Ranalli, 1995). The calculated creep viscosity is therefore limited in such manner:

$$\eta_{\text{creep}} \leq \frac{C + P \sin(\phi)}{(4\dot{\epsilon}_{II})^{1/2}} \quad (12)$$

where  $C$  is the cohesion and  $\phi$  is the internal angle of friction.

The Peierls mechanisms (Kameyama et al., 1999), or exponential creep, limits the strength of material at high pressure. This mechanism takes over from dislocation creep in areas of large stresses. The viscosity of a material flowing according to Peierls creep can be expressed in such manner

$$\eta_{\text{Peierls}} = \frac{1}{2 \times A_{\text{Peierls}} \times \sigma_{II}} e^{\left( \frac{E_a + PV_a}{RT} \times \left( 1 - \left( \frac{\sigma_{II}}{\sigma_{\text{Peierls}}} \right)^k \right)^q \right)} \quad (13)$$

where  $\sigma_{II}$  is the second stress invariant,  $\sigma_{\text{Peierls}}$  is a stress value that limits the strength of the material.  $A_{\text{Peierls}}$ ,  $k$ , and  $q$  are material constants derived from laboratory experiments which indicate that  $k$  should range between 0 and 1, and  $q$  should range between 1 and 2 for rocks (Kocks et al., 1975). In subduction modelling, slabs of olivine rheology are subject to large stresses and low temperature in contrast to the surrounding asthenosphere (Katayama and Karato, 2008). In this context Peierls creep is often activated at stresses which may be much lower than the material strength value,  $\sigma_{\text{Peierls}}$ .

Following the approach of coupled petrological-thermo-mechanical modelling (Gerya et al., 2006; Baumann et al., 2010), phase transitions are calculated at every timestep based on Gibbs free energy minimisation (Vasilyev et al., 2004). All local material properties such as density, heat capacity, thermal expansion, adiabatic and latent heating are calculated from thermodynamics in order to better constrain the effect of phase transitions on subduction processes.

Surface processes are implemented using a gross-scale erosion sedimentation law. In this approach, the interface crust/air or crust/water is tracked on a Eulerian grid. This surface evolves as an erosion/

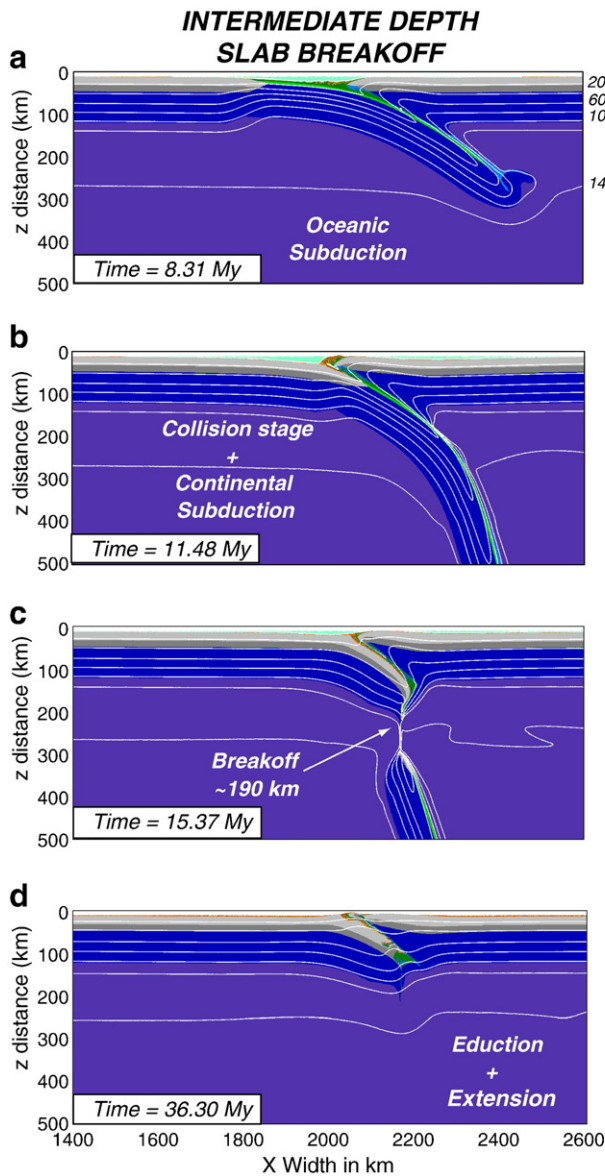


**Fig. 7.** Snapshots through the evolution of the intermediate depth slab breakoff member. a) Oceanic subduction. b) Continental collision and continental subduction. c) Breakoff d) Eduction and extension. Time is incremented from the start of the experiment. Origin of the  $z$  distance axis is the top of the box (including the 10 km thick air layer).

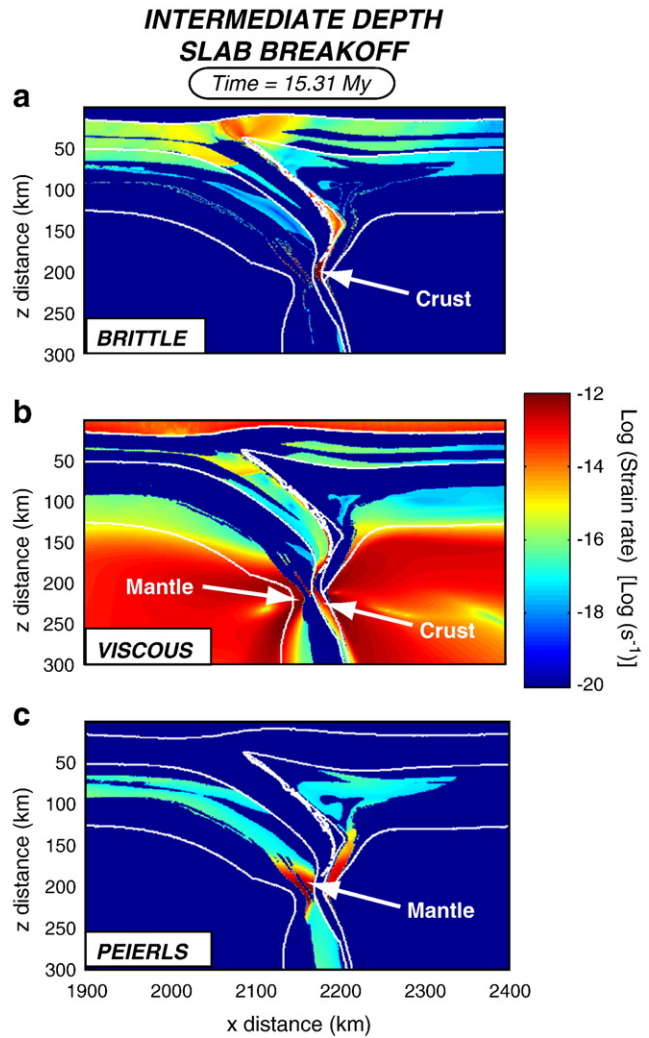


**Fig. 8.** Rheological mechanisms activated during intermediate depth slab breakoff. Brittle, viscous, and Peierls mechanism strain rates. At breakoff location, the crust deforms in a visco-plastic (brittle) manner and the mantle deforms both viscously and by Peierls mechanism. Dark blue means that mechanism is locally not activated during the process. Contours highlight interfaces between atmosphere, crust, mantle lithosphere and asthenosphere. Origin of the  $z$  distance axis is the top of the box (including the 10 km thick air layer).

sedimentation level according to the transport equation (Gerya and Yuen, 2003b)

$$\frac{\partial z_{es}}{\partial t} = v_z - v_x \frac{\partial z_{es}}{\partial x} - v_s + v_e \quad (14)$$

where  $z_{es}$  is the vertical position of the tracked interface,  $v_x$  and  $v_z$  are the material velocities interpolated on this interface,  $v_e$  and  $v_s$  are the gross-scale erosion/sedimentation rates defined with regard to a reference water level. Values used for this study are 0.1 mm/yr for both  $v_s$  and  $v_e$ .

2.2. Setup of the experiment

The experiments were performed in a 4000 × 1400 km box. The models used a grid resolution of 1361 × 351 nodes with variable grid spacing. This allowed a minimum grid resolution of 1 km in the area

subject to largest deformation. 13 million Lagrangian markers carrying material properties were used in each experiment. Two 1700 km long continental plates were separated by a 700 km long oceanic plate. Both continental plates and oceanic are composed of an upper crust, lower crust and lithospheric mantle (Fig. 1). The rheological parameters used in the experiments are presented in Table 2.

The boundary conditions used in this setup are free slip on all boundaries, except at the lower boundary which is treated as a permeable boundary satisfying an external free slip boundary condition (Burg and Gerya, 2005; Ueda et al., 2008). In order to let the topography build up, a free surface is simulated at the air/lithosphere interface by setting the viscosity of the air (10<sup>19</sup> Pa.s) to be at least two orders of magnitude lower than the crust (Schmeling et al., 2008). The thickness of the air layer used in the simulations was 10 km.

The thermal structure of the oceanic lithosphere was calculated from the half space cooling model for a given plate age (Turcotte and Schubert, 1982). The initial continental geotherm was set using values of 0 at the top and 1344 at the bottom of the lithosphere (140 km thick). The thermal gradient used within the asthenosphere was quasi-adiabatic (0.5/km).

In order to initiate subduction a weak zone was imposed on the right ocean–continent transition. The weak zone cuts through the whole lithospheric mantle with an angle of 30° and is characterised by weak plastic strength (1 MPa) and wet olivine rheological parameters

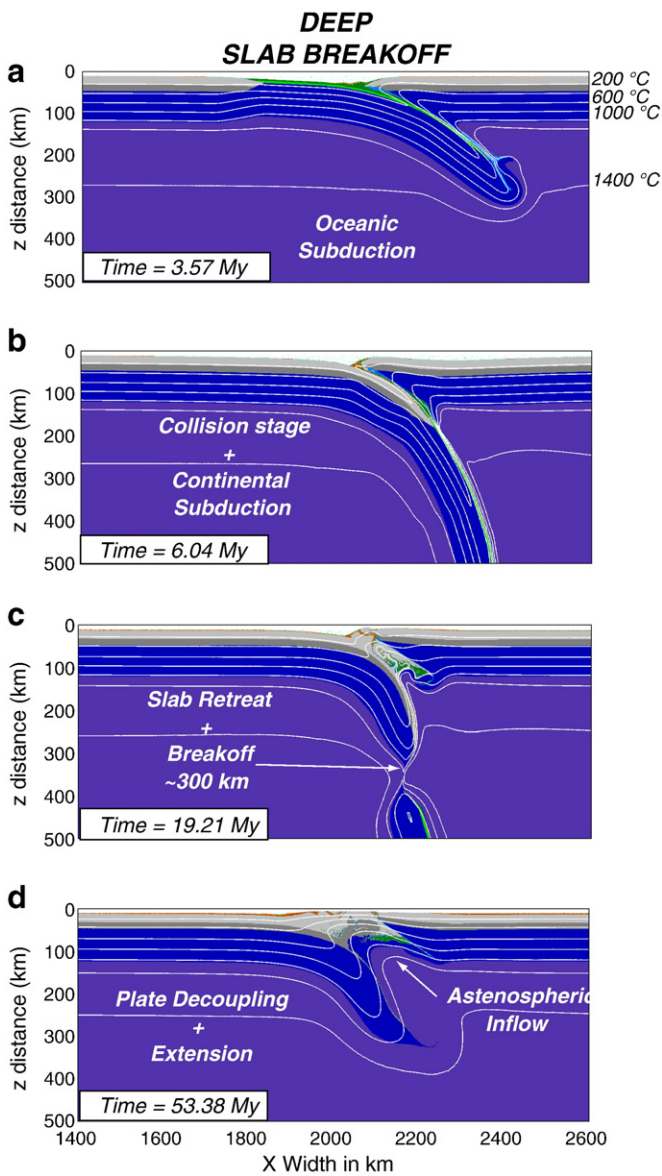


Fig. 9. Deep slab breakoff end-member evolution in four stages. a) Oceanic subduction. b) Continental collision and continental subduction. c) Slab retreat, breakoff and eduction d) Plate decoupling, rebound and extension. Time is incremented from the start of the experiment. Origin of the z distance axis is the top of the box (including the 10 km thick air layer).

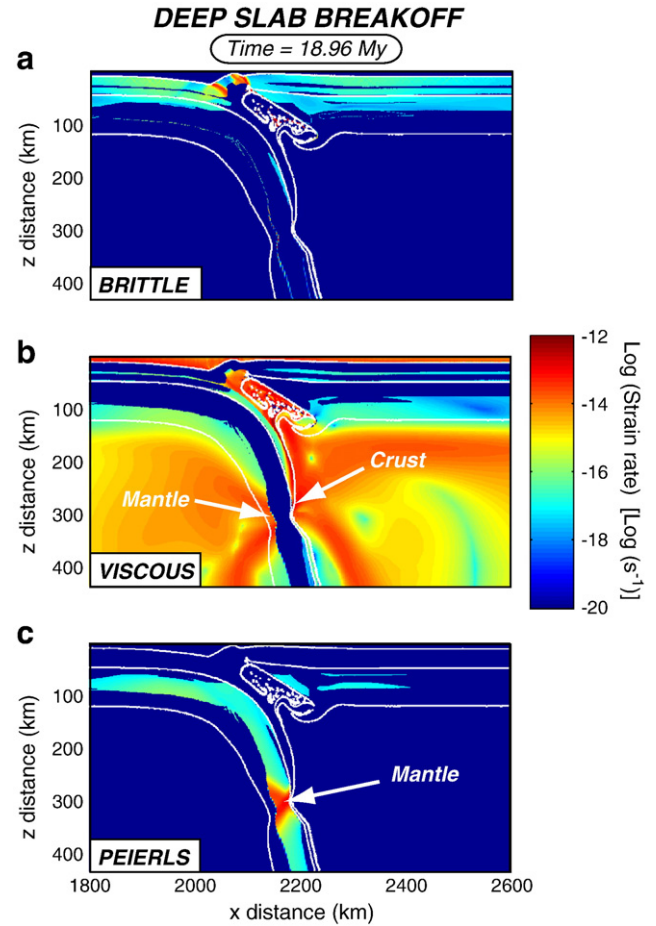


Fig. 10. Rheological mechanisms activated during deep slab breakoff. Brittle, viscous, and Peierls mechanism strain rates. In the necking zone, the crust deforms viscously and the mantle lithosphere deforms both viscously and by Peierls mechanism. Dark blue means that mechanism is locally not activated during the process. Contours highlight interfaces between atmosphere, crust, mantle lithosphere and asthenosphere.

(Ranalli, 1995). Despite the fact that subduction initiation can be modelled in a geologically more relevant manner (Gerya et al., 2008; Ueda et al., 2008; Nikolaeva et al., 2010), the use of such a weak zone remains useful for our specific setup.

A fixed convergence rate is imposed on both continental plates until 500 km of oceanic crust has been subducted, afterward, subduction and subsequent collision are only driven by slab pull.

### 3. Model results

In our study we systematically explored a two dimensional parameter space. The parameters which were varied are the original convergence rate of the plates which is applied until 500 km of convergence is reached and the age of the oceanic lithosphere (Fig. 2). The convergence rate is symmetric; each plate is pushed with the same constant velocity until 500 km of total convergence is reached. This enables us to reach a point where the weight of the hanging slab is heavy enough to drive the subduction–collision system. The age of the oceanic segment is constant along the plate, varying this parameter enables us to indirectly vary the original plate strength by modifying its initial temperature structure. By independently varying those parameters, we observed four different end-members of slab breakoff and model evolution. Those different end-members are characterised by different slab breakoff depths linked to activation of different rheological mechanisms. Each model exhibits a different post breakoff evolution which can be monitored in the evolution of the topographic signal. Results of the parametric study can be seen in

Fig. 2 where different modes of slab breakoff are displayed as a function of the varied parameters.

In all experiments, slab breakoff events can be identified by monitoring stresses in the slab. A slab detachment episode is responsible for a large stress drop within the slab (Fig. 16b) and a very sharp increase of the strain rate within the slab (Fig. 16c).

#### 3.1. Shallow slab breakoff

Our modelling results suggest that shallow slab detachment is likely to occur in young oceanic lithosphere (Fig. 3) with fast plate convergence rates. In this particular setting, fast breakoff takes place soon after the continental plates reach the collision stage (~1 My) and continental crust subduction does not develop. Detachment is localised at the ocean–continent transition and the depth of the rupture is very shallow (~40 km). Once the rupture is initiated, detachment of the oceanic lithosphere occurs along the subduction plane, triggering the opening of an asthenospheric window under the collision zone. Asthenospheric inflow at a subcrustal level may have some major consequences for magmatism and volcanism. Rheological mechanisms responsible for this mode of slab breakoff are viscous creep in the mantle lithosphere, whereas the crust behaves in a plastic (brittle) manner (Fig. 4).

The topographic evolution map (Fig. 11) displays a convergence stage with the formation of a deep trench and accretionary wedge. A collision signal can be observed as the topography reaches its peak value on the order of 2 km. This is the consequence of squeezing the

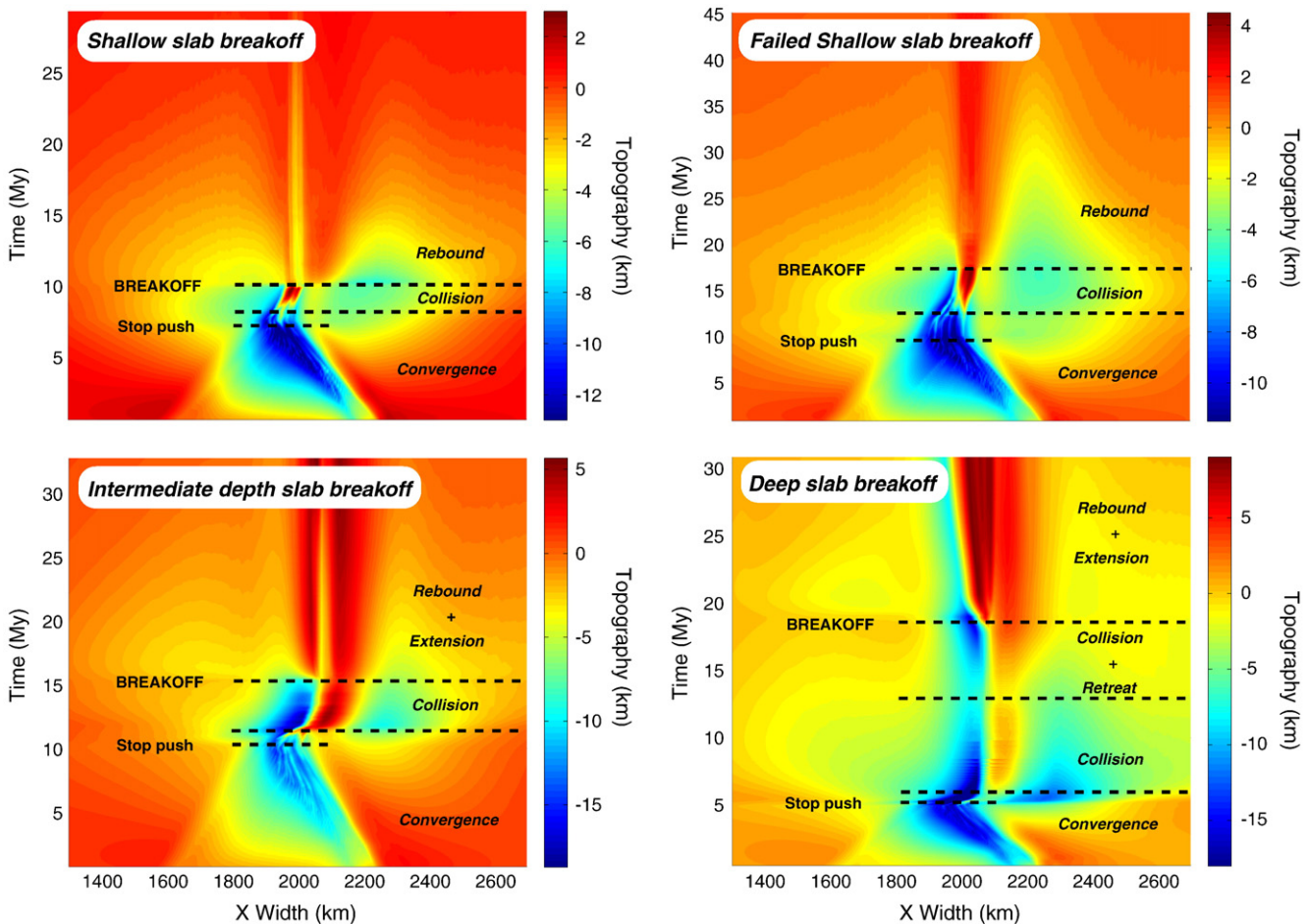


Fig. 11. Topography evolution through time above the subduction–collision zone for each end-member. For each case, a sharp breakoff signal and subsequent uplift is observed. The overall topographic signal can be divided in time windows corresponding to different geodynamic stages.

accretionary wedge between the colliding continental plates. After approximately 2 My, slab breakoff occurs and produces a sharp topographic signal. Extension related to the opening of the asthenospheric window produced a collapse of the topography. An uplift of few kilometres (~4 km) related to breakoff is recorded above the former subduction zone. The topographic response is fast (~5 My) which produces an average uplift rate of 0.8 mm/yr. Finally, the system stabilises and surface processes tend to flatten out the topography over a long timescale (~15 My).

### 3.2. Failed shallow slab breakoff

Using a slow initial total convergence rate (2.5 cm/yr), a second end-member of young oceanic slab breakoff was observed (Fig. 5). In this particular case, breakoff does not localise at the ocean–continent transition, but instead occurs at a much deeper level (~400 km). As in the shallow breakoff mode, convergence stops after both continental plates meet, the weight of the hanging slab is not sufficient to overcome the buoyancy of continental crust. As the convergence velocity was originally slow, the subducted slab is hotter (i.e. both less strong and less dense) and extensional stresses are not high enough to cause a shallow slab rupture. Similar bifurcation with sharp changes in the slab detachment depth was also observed in previous breakoff models with relatively warm slabs (Gerya et al., 2004). Detachment occurs approximately 5 My after the termination of subduction (Fig. 6) the main deformation mechanism activated during the breakoff was viscous creep.

The topographic evolution shows similarities with the fast shallow breakoff mode (Fig. 11). Topography reaches its peak value during the collision stage (~4 km). The slab breakoff topographic signal is more diffuse than in the fast shallow breakoff mode but post breakoff uplift last longer (~20 My) and uplift rates are on the order of 0.2 mm/yr. In each of those breakoff end-members involving young oceanic slabs, the topography after breakoff is relatively low and the width of the orogen is narrow (~100 km).

### 3.3. Intermediate depth slab breakoff

Models involving an oceanic lithosphere older than 30 My and with total convergence rates faster than 2.5 cm/yr display significantly different behaviour (Fig. 7). In this case, the oceanic lithosphere is dense enough to initiate continental crust subduction and strong enough not to yield before the buoyant crust is subducted deep enough. Breakoff occurs at the ocean–continent transition a few million years after the collision stage initiated (~4 My). The rupture occurs at the depth of approximately 200 km during the stage of slab steepening. The rupture is due to the combined action of viscous creep in the hotter crust and mantle of the two outer layers of the slab and Peierls mechanism in the cold mantle lithosphere of the slab core (Fig. 8). As soon as breakoff ends, the orogen undergoes a short period of extension, coeval with eduction of the buoyant continental crust (Andersen et al., 1991).

The topographic signal shows distinct signals for convergence, collision, slab breakoff and subsequent rebound (Fig. 11). Trench depth notably increases and reaches a rather unrealistic peak value greater than 10 km. During the collision stage, the overriding plate displayed positive topography of ~4 km in height. Post breakoff rebound linked to the eduction triggered the formation of positive topography on the subducted plate and further disappearance of the trench. The uplift rate is 0.5 mm/yr with a rebound of 5 km in approximately 10 My. Topography on both side of the suture reached a value of ~4 km in height. Finally, the width of the orogen reached ~300 km.

### 3.4. Deep slab breakoff

By using an oceanic lithosphere of age greater than 60 My for any convergence rate, or using a younger oceanic lithosphere with slow

convergence rate, deep slab breakoff was observed (Fig. 9). For this end-member, the depth of the detachment is above 250 km deep and breakoff can occur around 10 My after the start of collision. The strong and dense slab is able to drag down the continental crust to a depth above 200 km before detachment occurs at the ocean–continent transition. Prolonged slab steepening initiates plate decoupling and slab retreat. Breakoff occurs during slab retreat in a pure shear manner at the ocean–continent transition. The rupture is triggered by a complex activation of viscous creep (hot outer slab layers) and Peierls mechanism (colder slab core) in the mantle lithosphere and viscous creep in the crust (Fig. 10). A short episode of eduction was observed after breakoff but eduction is not the dominant exhumation mechanism in this model. Plate decoupling triggers the exhumation of the buoyant crustal material in the subduction channel and the opening of an asthenospheric window under the orogen.

The evolution of topography above the orogen is mostly similar to the intermediate depth breakoff end-member (Fig. 11). The main differences are the prolonged collision stage before breakoff and the post breakoff evolution. As the plates are decoupled, the orogen is free to undergo large scale extension after slab detachment. The uplift rate is 0.2 mm/yr with an uplift of 2 km in 10 My. Most of the topography is accommodated on the subducted plate during extension, with a maximum topography greater than 5 km in height. Total width of the orogen reaches 400 km at this stage.

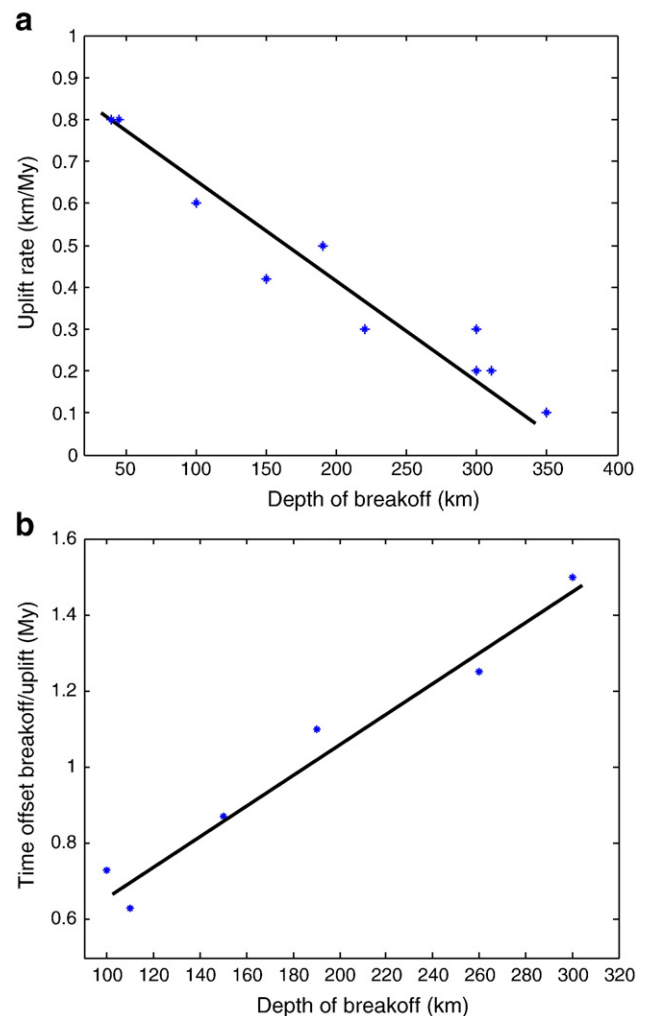


Fig. 12. a) Correlation between average uplift rate in the foreland basin and breakoff depth. Uplift rates are averaged over the 5 My following slab breakoff. b) Time delay between slab detachment and breakoff depth.

## 4. Discussion

### 4.1. Modelled and observed surface uplift rates

A strong correlation between average uplift rates and depth of breakoff was observed in the experiments. Fast uplift rates can be expected in the case of shallow slab detachment whereas deeper detachment provides slower uplift rates. The magnitude of the modelled uplift rates ranged from 0.8 to 0.1 mm/yr (Fig. 12a). Geological and geophysical studies suggest natural prototypes where uplift is related to slab breakoff. Such uplift rates are estimated around 0.3 mm/yr in Borneo (Morley and Back, 2008) and 0.25–0.5 mm/yr in Central America (Rogers et al., 2002). Those measurements are consistent with uplift rates calculated in our study. According to the surface processes parameters used in the simulations, comparing modelled uplift rates and measured uplift rates may give additional information on the depth and timing of slab detachment in the studied areas. A relation between the time of breakoff and the start of the post breakoff uplift has also been observed in our simulations (Fig. 12b). This time offset is strongly dependent on the depth of slab detachment and it decreases as the depth of breakoff decreases.

### 4.2. Rheology of the lower crust

The rheology of the lower crust plays a crucial role on the ability of the crust to support topography (Clark et al., 2005). In our parametric study, we considered a rather strong lower continental crust of

plagioclase rheology (An75 from (Ranalli, 1995)). By using of a weaker material (quartzite flow law) to simulate lower crust, comparable simulations would produce smoother topography. Fig. 13 shows a comparison between two intermediate depth breakoff models, one including a plagioclase lower crust and the other including a quartzite lower crust. The model including a quartzite lower crust display a broader orogen before and after slab detachment. Using a weak lower crust enables the building of topography on the lower plate during subduction, less crustal material is entrained in the subduction channel. This has the consequence to weaken the slab and therefore detachment occurs earlier ( $\sim 2$  My) and shallower ( $\sim 20$  km) than in the models including a plagioclase lower crust. The weak lower crust induces a slower but broader topographic response on the lower plate. Slower rates may be related to the fact that the response is rather distributed (broader) on a weaker crust.

### 4.3. Importance of Peierls mechanism

In contrast to previous slab breakoff studies using the I2VIS numerical code (Gerya et al., 2004; Baumann et al., 2010), this study includes the effects of Peierls mechanism which brings us closer to natural processes. Activation of Peierls mechanism by large extensional stresses in the cold core of the hanging slab is of first order importance for slab breakoff modelling. Drastic discrepancies were observed between similar model setups in which the only difference was the inclusion of Peierls mechanism. Timing and depth of breakoff, along with the topography were also different. In Fig. 14, a model including Peierls mechanism show faster ( $\sim 10$  My) and shallower

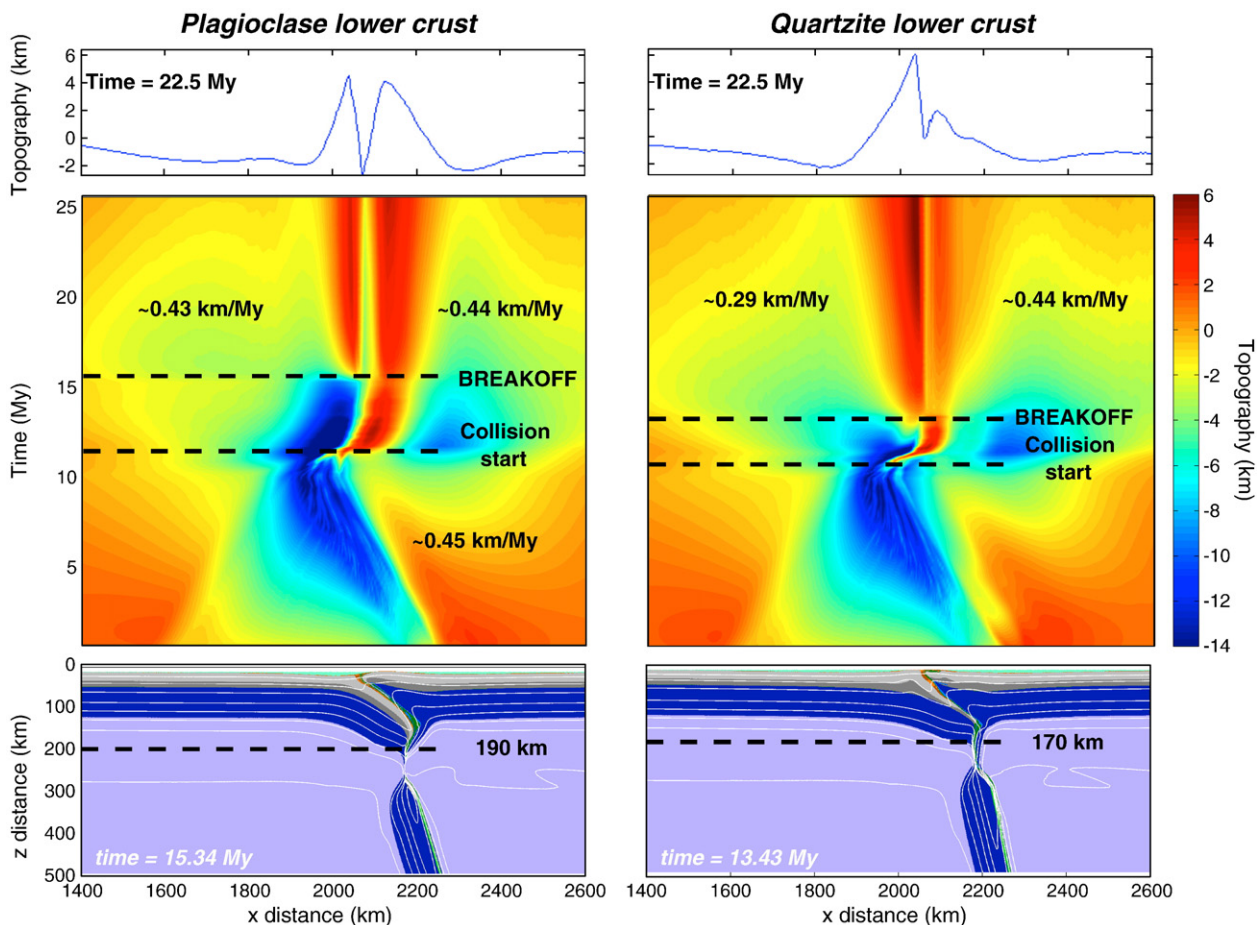
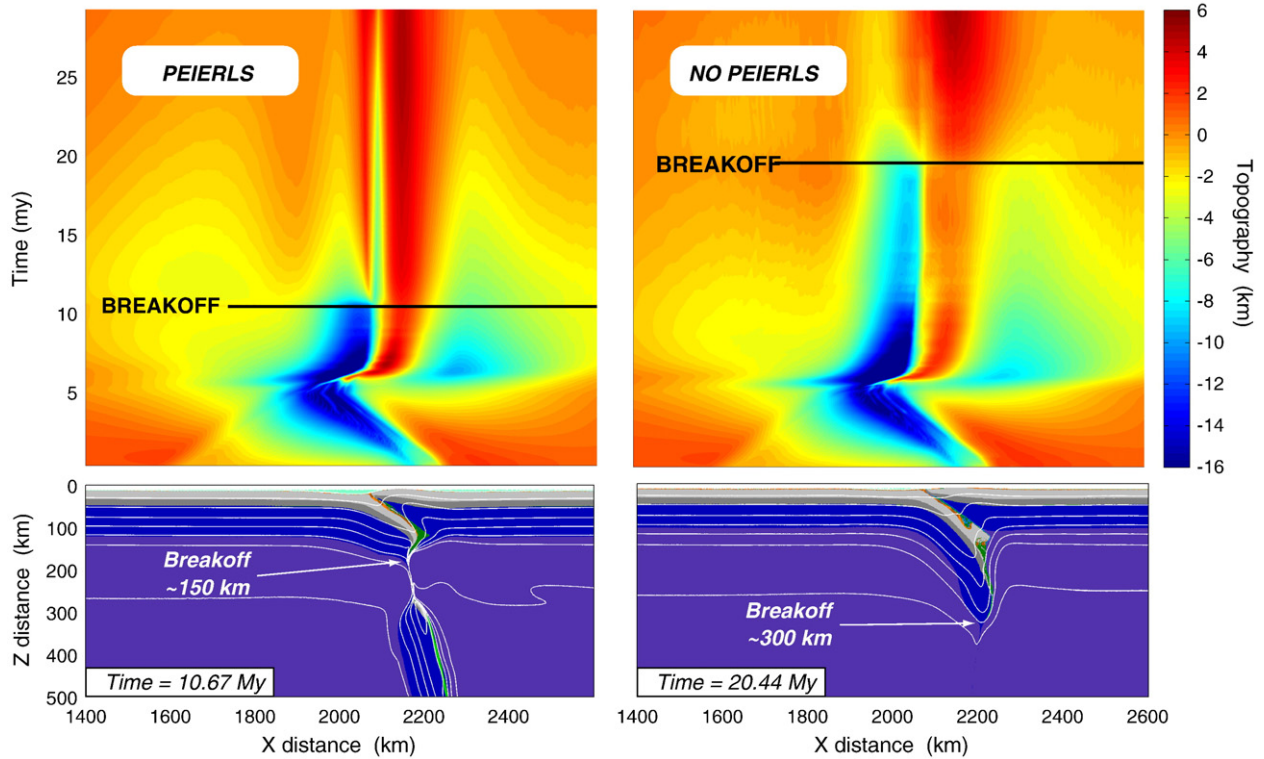


Fig. 13. Comparison of the intermediate depth breakoff end-member using plagioclase and quartzite flow law for lower crust rheology. The colormaps display the topographic evolution of each model. The cross-section display phases distribution at breakoff time. The upper plots display topographic profiles for each model, 22.5 My after the start of the simulation. Thick dashed line indicates timing of initiation of collision and timing of breakoff. Time is incremented from the start of the simulation.



**Fig. 14.** Comparison between models with and without Peierls mechanism. Parameters used in this setup are an oceanic lithosphere age of 40 My and initial total plate rate of 10 cm/y. Origin of the z distance axis is the top of the box (including the 10 km thick air layer).

breakoff. Topography evolution starts differing ~10 My after the start of the experiment. Late orogenic development and the final geometry are also strongly affected.

#### 4.4. Metastability of olivine

As our petrological approach is based on Gibbs energy minimisation, the experiments do not take into account the potential effect of metastable reactions. Schmeling et al. (1999) discussed the importance of metastable olivine in subducting slab. In their experiments, old slabs can potentially contain a significant volume of metastable olivine on the prograde path. A buoyant olivine wedge has a tendency to slow down subduction, hence influencing the dynamics. Subduction slowdown is regarded as one of the mechanism triggering slab detachment (Li and Liao, 2002). Although it is not clear that slabs contain large amount of metastable olivine, its buoyant effect may influence both depth and timing of slab breakoff.

#### 4.5. Orogenic evolution and exhumation mechanisms

In our study, subduction–collision models involving an oceanic crust older than 30 My are likely to trigger continental crust subduction. Intermediate depth and deep slab breakoff end-members are likely to occur for such slab ages. Both of these end-members display different exhumation mechanisms, namely a coherent crustal nappe exhumation due to eduction and buoyant flow of subducted crust triggered by slab retreat (Fig. 15). In our experiments, both eduction and rollback require subduction of a significantly long oceanic slab (~400 km) before the onset of collision.

- For deep slab breakoff, slab steepening initiates plate decoupling and slab retreat, triggering exhumation of the crust in a buoyant flow manner. In this case, exhumation is likely to start before breakoff. Models involving old oceanic lithosphere develop

complete plate decoupling and inflow of asthenospheric material at a shallow level (Fig. 9) and undergo a major topography building phase during post breakoff extension (Fig. 11).

- For intermediate depth breakoff, rupture occurs during slab steepening and thus prevents further steepening to trigger slab retreat and plate decoupling. Once breakoff ends, exhumation of the subducted crust occurs along the subduction plane with a normal sense motion. This mechanism is known as eduction and has already been suggested to explain the exhumation of UHP rocks (Andersen et al., 1991).

#### 4.6. Evolution of stresses in the lithosphere

A slab detachment event is responsible for a stress redistribution within the lithosphere. This can be observed in Fig. 16a which shows the stress distribution within the model lithosphere before and after breakoff. Release of the gravitational stresses during breakoff is followed by an increase of stress in the lower plate. This increase of stress is related to the positive buoyancy of the subducted continental crust which is no longer driven down by the slab. The increase of stress is controlled by the amount of eduction as this mechanism allows, to some extent, the exhumation of the buoyant crust. An overall increase of stress (lower and overriding plate) is also noticeable in the crustal part of the model which is subject to topography building and loading.

#### 4.7. Comparison with preceding studies

In comparison with preceding studies (Davies and von Blanckenburg, 1995; Li and Liao, 2002), we do not observe a systematic correlation between the initial plate rate, or the subduction velocity, and depth of slab detachment. The influence of the initial plate rate is clearly noticeable for young slabs, where a sharp transition between shallow and failed shallow breakoff occurs for initial plate rate lower than 5 cm/yr. For older slabs, depth of detachment does not show such a clear dependence on the

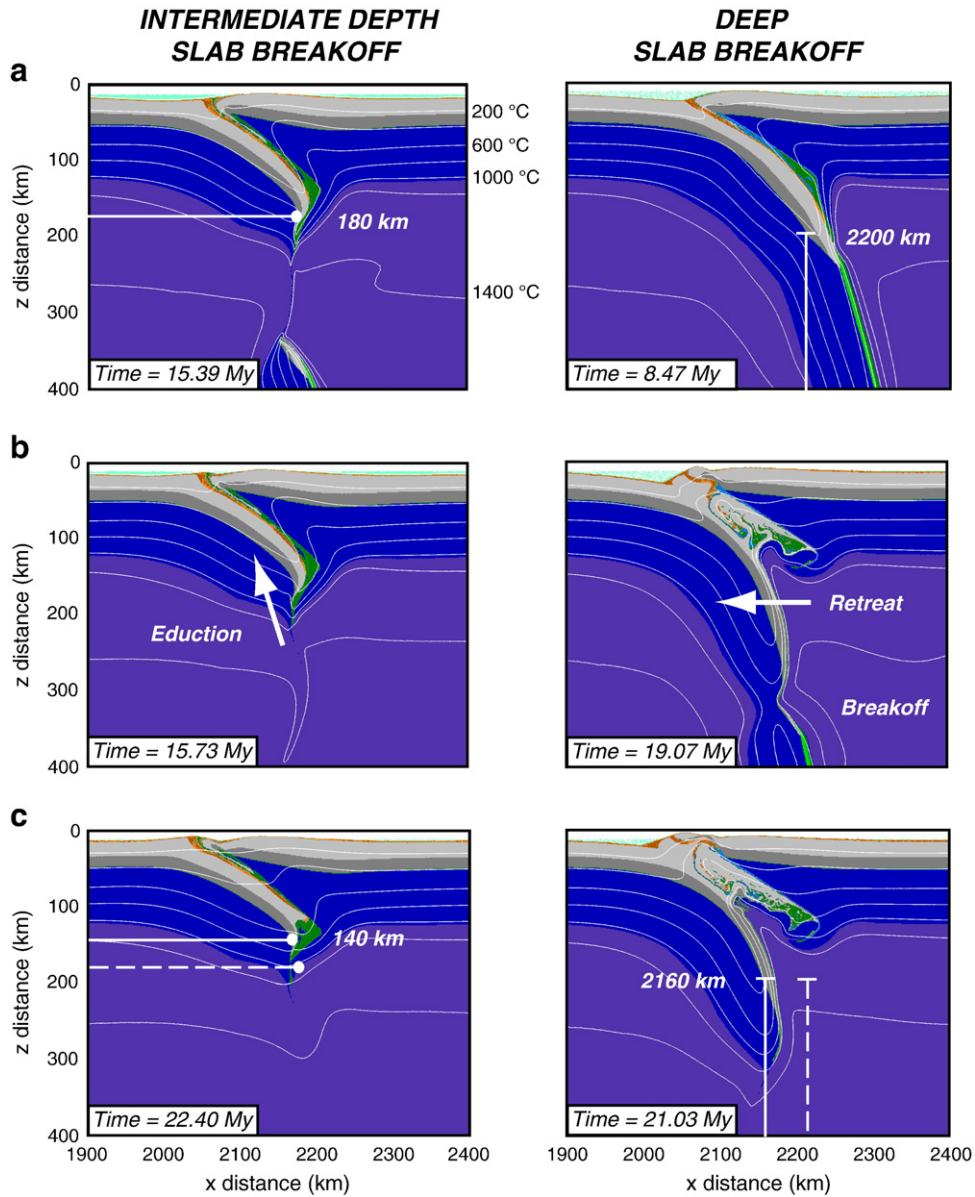


**Fig. 15.** Contrasting exhumation styles for intermediate depth and deep slab breakoff. Exhumation of continental crust is responsible for most of the exhumation in the case of intermediate depth end-member whereas buoyant crustal flow is triggered by slab retreat in the case of deep slab breakoff. Time is incremented from the start of the experiment. Origin of the z distance axis is the top of the box (including the 10 km thick air layer).

initial convergence rate since different breakoff modes can affect slabs of the same age but with a different initial plate rate.

In our study, shallow slab breakoff displays comparable results with [van de Zedde and Wortel \(2001\)](#) in which asthenospheric material can rise up to subcrustal depths. However, in our case, it does not necessarily require continental crust subduction or a slow convergence rate as the failed shallow slab breakoff mode can take over if the initial convergence rate is too slow (less than 7.5 cm/yr).

Intermediate depth slab breakoff displays the same breakoff depths and occurs on the same timescale (5–7 My after stopping the convergence) as the shallow plastic breakoff in [Andrews and Billen \(2009\)](#), despite the fact that they do not utilise the same rheological mechanisms and that initial setups differs from the one used here.

Our deep breakoff depth is comparable to the deep viscous breakoff in [Andrews and Billen \(2009\)](#). However, in our models the timing of rupture is shorter (10–20 My) than in their experiments (15 to 25) for slabs of the same age. This is likely due to the activation of Peierls mechanisms in the mantle lithosphere which enables breakoff to occur earlier ([Fig. 14](#)).

Rheological mechanisms responsible for slab breakoff are different for each type of end-member as suggested by [Andrews and Billen \(2009\)](#), with the exception of the failed shallow slab breakoff end-member in which many deformation mechanisms are likely to be activated during the rupture. Plastic behaviour (Druker–Prager) is only important for shallow slab breakoff however this only affects the crust. Peierls appears to be a key mechanism for slab breakoff dynamics ([Fig. 14](#)). This mechanism plays an important in the mantle lithosphere for intermediate depth and slab breakoff.

Fluid/melt related weakening effects are not taken into account in this study, however they can potentially have a strong influence on the mechanism of breakoff and the overall orogenic evolution. [Faccenda et al. \(2009\)](#) discuss the influence of fluid percolation on the orogenic style (coupled or decoupled plates). In our models, despite the lack of fluids, we observe both coupled and decoupled orogens. Plate decoupling (slab retreat) occurs in the case of old slabs (80 My) which are dense, but strong enough to initiate a rollback event before breakoff. Including the effect of fluids may drastically enhance the amount of rollback.

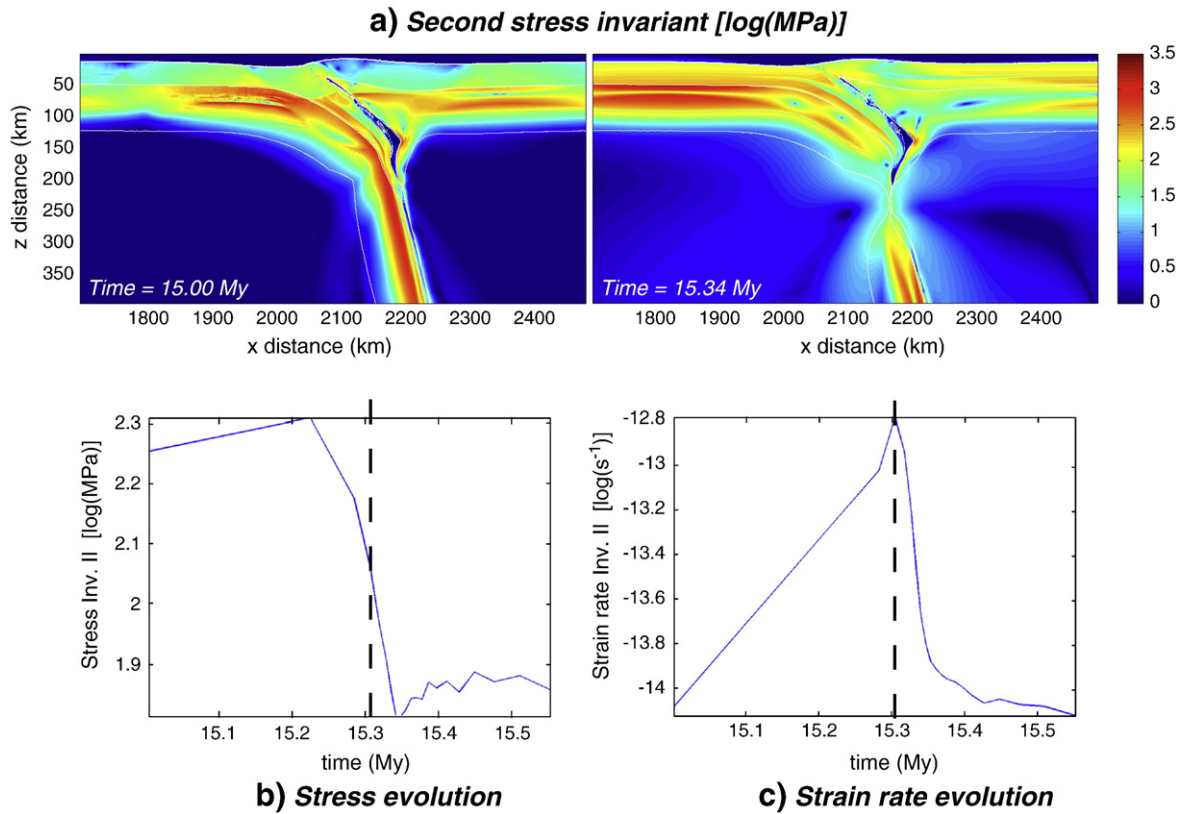


**Fig. 16.** a) Second stress invariant map before and after slab detachment. Contours highlight interfaces between atmosphere, crust, mantle lithosphere and asthenosphere. b) Evolution of the average stress (second invariant) in the slab necking zone through time. The dashed line indicates the breakoff event. c) Evolution of the average strain rate (second invariant) in the slab necking zone through time. The dashed line indicates the breakoff event. Time is incremented from the start of the simulation.

In our study we frequently observed a deep topography at the subduction trench. Trench depths larger than 10 km are not representative of present-day Earth subduction zones. This effect might be related to the fact that modelling approach employed a visco-plastic rheology, which does not include the effects of elasticity. Including a visco-elasto-plastic rheology enables the production of more realistic topographic profiles throughout subduction simulations (Sobolev and Babeyko, 2005).

#### 4.8. Possible application to natural prototypes

Different modes of slab breakoff can be identified. They are characterised by the depth of breakoff, timing of the detachment, activation of different rheological mechanisms, style of topographic evolution and orogenic development. These end-members can potentially be applied to many natural prototypes where surface observables such as uplift rates or heatflow can be measured and where the geophysical data such as tomography or hypocenter location supports the possibility of slab breakoff.

Areas such as Eastern Anatolia (Turkey) where magmatism witnesses from deep heating and where mantle lithosphere is shallow to absent (Keskin, 2003) would favour the possibility of shallow slab breakoff. On the other hand, large orogens such as Caledonides where breakoff and exhumation were suggested as a possible mechanism of UHP rocks exhumation (Andersen et al., 1991) would rather favour an intermediate or deep slab breakoff scenario.

## 5. Conclusions

Our modelling study provides a wide range of topographic behaviour linked to different slab breakoff end-members. The study takes into account a more realistic complex rheology which includes

Peierls mechanisms. This mechanism turns out to play an important role for the depth and timing of slab detachment and is an important deformation mechanism for several breakoff end-member.

The four different slab breakoff modes display significantly different topographic development. The evolution of the models involves different geodynamic processes such as slab steepening or retreat and slab breakoff is responsible for the sharpest signal in the topography evolution.

A correlation between the depth of detachment and the surface uplift rate recorded in the foreland and hinterland basins has been observed; the shallower the breakoff is, the faster the uplift rate will be. In our context, exhumation of subducted buoyant crust can occur by either slab retreat and buoyant flow of crust in the extending subduction channel or by coherent exhumation of deeply subducted continental plate.

## Acknowledgments

The manuscript has been improved by comments from Sierd Cloetingh and two anonymous reviewers. Boris Kaus, Laetitia Iku Le Pourhiet, Philippe Jun Yamato, and Stefan Schmalholz are thanked for stimulating discussions. This study was supported by SNF-EU research grant 20TO21-120535 (TOPO-4D). All the simulations were run on the ETH Brutus cluster.

## References

- Andersen, T.B., Jamtveit, B., Dewey, J.F., 1991. Subduction and exhumation of continental crust: major mechanisms during continent-continent collision and orogenic extensional collapse, a model based on the south Norwegian Caledonides. *Terra Nova* 3 (3), 303–310.
- Andrews, E.R., Billen, M.I., 2009. Rheologic controls on the dynamics of slab detachment. *Tectonophysics* 464 (1–4), 60–69.

- Baumann, C., Gerya, T.V., Connolly, J.A.D., 2010. Numerical modelling of sponaneous slab breakoff dynamics during continental collision. In: Spalla, M., Marotta, A., Gosso, G. (Eds.), *Advances in Interpretation of Geological Processes: Refinement of Multi-Scale Data and Integration in Numerical Modelling*. Geological Society of London Special Publication., Vol. 322. Geological Society, London, pp. 99–114.
- Buiter, S.J.H., Govers, R., Wortel, M.J.R., 2002. Two-dimensional simulation of surface deformation caused by slab detachment. *Tectonophysics* 354 (3–4), 192–210.
- Burg, J.P., Gerya, T.V., 2005. The role of viscous heating in Barrovian metamorphism of collisional orogens: thermomechanical models and application to the Lepontine Dome in the Central Alps. *Journal of Metamorphic Geology* 23, 79–95.
- Chen, W.-P., Brudzinski, M.R., 2001. Evidence for a large-scale remnant of subducted lithosphere beneath Fiji. *Science* 292, 2475–2479.
- Clark, M., Bush, J., Royden, L., 2005. Dynamic topography produced by lower crustal flow against rheological strength heterogeneities bordering the Tibetan plateau. *Geophysical Journal International* 162 (2), 575–590.
- Clauser, C., Huenges, E., 1995. Thermal conductivity of rocks and minerals. In: Ahrens, T.J. (Ed.), *Rock Physics and Phase Relations*. AGU, AGU reference shelf 3, Washington DC, pp. 105–126.
- Cloetingh, S., Burov, E., Matenco, L., Toussaint, G., Bertotti, G., Andriessen, P., Wortel, M., Spakman, W., 2004. Thermo-mechanical controls on the mode of continental collision in the SE Carpathians (Romania). *Earth and Planetary Science Letters* 218, 57–76.
- Davies, H.J., von Blanckenburg, F., 1995. Slab breakoff: a model of lithosphere detachment and its test in the magmatism and deformation of collisional orogens. *Earth and Planetary Science Letters* 129 (1–4), 85–102.
- Evans, B., Goetze, C., 1979. Temperature variation of hardness of olivine and its implication for polycrystalline yield stress. *Journal of Geophysical Research* 84, 5505–5524.
- Faccenna, M., Minelli, G., Gerya, T., 2009. Numerical modeling of active advancing and retreating post-subduction collision controlled by rheological weakening of the subduction channel. *Earth and Planetary Science Letters* 278 (3–4), 337–349.
- Ferrari, L., 2004. Slab detachment control on mafic volcanic pulse and mantle heterogeneity in central Mexico. *Geology* 32 (1), 77–80.
- Gerya, T.V., Yuen, D.A., 2003a. Characteristic-based marker method with conservative finite-difference schemes for modeling geological flows with strongly variable transport properties. *Physics of the Earth and Planetary Interiors* 140 (4), 293–318.
- Gerya, T.V., Yuen, D.A., 2003b. Rayleigh–Taylor instabilities from hydration and melting propel 'cold plumes' at subduction zones. *Earth and Planetary Science Letters* 212 (1–2), 47–62.
- Gerya, T.V., Yuen, D.A., Maresch, W., 2004. Thermomechanical modelling of slab detachment. *Earth and Planetary Science Letters* 226 (1–2), 101–116.
- Gerya, T.V., Connolly, J.A.D., Yuen, D.A., Górczyk, W., Capel, A.M., 2006. Seismic implications of mantle wedge plumes. *Physics of the Earth and Planetary Interiors* 156 (1–2), 59–74.
- Gerya, T.V., Connolly, J.A.D., Yuen, D.A., 2008. Why is terrestrial subduction one-sided? *Geology* 36 (1), 43–46.
- Kameyama, M., Yuen, D.A., Karato, S.-I., 1999. Thermal–mechanical effects of low-temperature plasticity (the peierls mechanism) on the deformation of viscoelastic shear zone. *Earth and Planetary Science Letters* 168 (1–2), 159–172.
- Katayama, I., Karato, S.-I., 2008. Rheological structure and deformation of subducted slabs in the mantle transition zone: implications for mantle circulation and deep earthquakes. *Physics of the Earth and Planetary Interiors* 168 (3–4), 125–133.
- Keskin, M., 2003. Magma generation by slab steepening and breakoff beneath subduction–accretion complex: an alternative model for collision-related volcanism in Eastern Anatolia, Turkey. *Geophysical Research Letters* 30 (24), 1–4.
- Kocks, U.F., Argon, A.S., Ashby, M.F., 1975. Thermodynamics and kinetics of slip. *Progress in Materials Science* 19, 1–281.
- Li, L., Liao, X., 2002. Slab breakoff depth: a slowdown subduction model. *Geophysical Research Letters* 29 (3), 1–3.
- Macera, P., Gasperini, D., Ranalli, G., Mahatsente, R., 2008. Slab detachment and mantle plume upwelling in subduction zones: an example from the Italian South–Eastern Alps. *Journal of Geodynamics* 45 (1), 32–48.
- Morley, C.K., Back, S., 2008. Estimating hinterland uplift exhumation from late orogenic basin volume, NW Borneo. *Journal of the Geological Society* 165, 353–366.
- Nikolaeva, K., Gerya, T., Marques, F., 2010. Subduction initiation at passive margins: numerical modeling. *Journal of Geophysical Research* 115.
- Qin, J., Lao, S., Li, Y., 2008. Slab breakoff model for the Triassic post-collisional adakitic granitoids in the Qinling Orogen, Central China: zircon U–Pb Ages, geochemistry, and Sr–Nd–Pb isotopic constraints. *International Geology Review* 50, 1080–1104.
- Ranalli, G., 1995. *Rheology of the Earth*, 2nd ed. Chapman & Hall, London.
- Regard, V., Faccenna, C., Bellier, O., Martinod, J., 2008. Laboratory experiments of slab break-off and slab dip reversal: insight into the Alpine Oligocene reorganization. *Terra Nova* 20 (4), 267–273.
- Rogers, R.D., Karason, H., van der Hilst, R.D., 2002. Epeirogenic uplift above a detached slab in northern Central America. *Geology* 30, 1031–1034.
- Schmeling, H., Monz, R., Rubie, D., 1999. The influence of olivine metastability on the dynamics of subduction. *Earth and Planetary Science Letters* 165 (1), 55–66.
- Schmeling, H., Babeyko, A.Y., Enns, A., Faccenna, C., Funicello, F., Gerya, T.V., Golabek, G.J., Grigull, S., Kaus, B.J.P., Morra, G., Schmalholz, S.M., van Hunen, J., 2008. A benchmark comparison of spontaneous subduction model—towards a free surface. *Physics of the Earth and Planetary Interiors* 171 (3–4), 198–224.
- Sobolev, S.V., Babeyko, A.Y., 2005. What drives orogeny in the Andes? *Geology* 33 (8), 617–620.
- Sperner, B., Lorenz, F., Bonjer, K., Hettel, S., Müller, B., Wenzel, F., 2001. Slab break-off—abrupt cut or gradual detachment? New insights from the Vrancea Region (SE Carpathians, Romania). *Terra Nova* 13 (3) 172–139.
- Ton, S.W.A., Wortel, M., 1997. Slab detachment in continental collision zones: an analysis of controlling parameters. *Geophysical Research Letters* 24 (16), 2095–2098.
- Toussaint, G., Burov, E., Jolivet, L., 2004. Continental plate collision: unstable vs. stable slab dynamics. *Geology* 32 (1), 33–36.
- Turcotte, D.L., Schubert, G., 1982. *Geodynamics: Application of Continuum Physics to Geological Problems*. John Wiley, New York.
- Ueda, K., Gerya, T., Sobolev, S.V., 2008. Subduction initiation by thermal–chemical plumes: numerical studies. *Physics of the Earth and Planetary Interiors* 171 (1–4), 296–312.
- van de Zedde, D.M.A., Wortel, M.J.R., 2001. Shallow slab detachment as a transient source of heat at midlithospheric depths. *Tectonics* 20 (6), 868–882.
- Vasilyev, O.V., Gerya, T., Yuen, D.A., 2004. The application of multidimensional wavelets to unveiling multi-phase diagrams and in-situ physical properties of rocks. *Earth and Planetary Science Letters* 223, 49–64.
- Wilmsen, M., Fürsich, F., Seyed-Emmani, K., Majidifard, M.R., Taheri, J., 2009. The Cimmerian Orogeny in northern Iran/ tectono-stratigraphic evidence in the foreland. *Terra Nova* 21 (3), 211–218.
- Wortel, M.J.R., Spakman, W., 2000. Subduction and slab detachment in the Mediterranean–Carpathian Region. *Science* 290, 1910–1917.